

Studying Distant Infrared–Luminous Galaxies with *Spitzer* and *Hubble*

By CASEY PAPOVICH, EIICHI EGAMI,
 EMERIC LE FLOC'H, PABLO PÉREZ-GONZÁLEZ,
 GEORGE RIEKE, JANE RIGBY, HERVÉ DOLE,
 AND MARCIA RIEKE

Steward Observatory, University of Arizona, 933 N. Cherry Avenue, Tucson, AZ 85741, USA

New surveys with the *Spitzer* space telescope identify distant star-forming and active galaxies by their strong emission at far-infrared wavelengths, which provides strong constraints on these galaxies' bolometric energy. Using early results from *Spitzer* surveys at 24 μm , we argue that the faint sources correspond to the existence of a population of infrared-luminous galaxies at $z \gtrsim 1$ that are not expected from predictions based on previous observations from *ISO* and *IRAS*. Combining *Spitzer* images with deep ground-based optical and *Hubble* Space Telescope imaging, we discuss the properties of galaxies selected at 24 μm in the region of the *Chandra* Deep Field South, including redshift and morphological distributions. Galaxies with $z \lesssim 1$ constitute roughly half of the faint 24 μm sources. Infrared-luminous galaxies at these redshifts span a wide variety of normal to strongly interacting/merging morphologies, which suggests that a range of mechanisms produce infrared activity. Large-area, joint surveys between *Spitzer* and *HST* are needed to understand the complex relation between galaxy morphology, structure, environment and activity level, and how this evolves with cosmic time. We briefly discuss strategies for constructing surveys to maximize the legacy of these missions.

1. Introduction

Infrared (IR) luminous galaxies represent highly active stages in galaxy evolution that are not generally inferred in optically selected galaxy surveys (e.g. Rieke & Low 1972; Soifer, Neugebauer, & Houck 1987). High IR-emission is typically generated in heavily enshrouded starbursts associated with morphologically disturbed or merging galaxies (Sanders *et al.* 1988); in comparison, optical studies probe less obscured star-forming regions often located in galaxy disks (e.g. Kennicutt 1998). At the present day, most of the light emitted from galaxies comes at optical wavelengths, with only one-third of the bolometric luminosity density coming in the IR (Soifer & Neugebauer 1991). However, the cosmic background implies that the far-IR emission from galaxies in the early Universe is as important energetically as the emission in the optical and UV combined (Hauser *et al.* 1998), and IR number counts from *ISO* indicate that these sources evolved faster than that inferred directly from UV/optical observations. The interpretation of these counts combined with models of the cosmic IR background (Elbaz *et al.* 2002; Dole *et al.* 2003) argues that IR-luminous stages of galaxy evolution were frequently more common at high redshift. As a result, IR-luminous galaxies may be responsible for a substantial fraction of the global star-formation and metal-production rate (e.g. Franceschini *et al.* 2001).

Studying the mechanisms for this apparent rapidly evolving IR-luminous galaxy population has been problematic, primarily due to low-number statistics of sources at high redshifts, and difficulty in measuring their multi-wavelength properties and internal structure. The improvements in IR sensitivity and survey efficiency now possible with *Spitzer* allow major advances in the study of the IR-luminous stages of galaxy evolution, particularly in true panchromatic datasets. Measurements at 24 μm with the *Spitzer*/MIPS

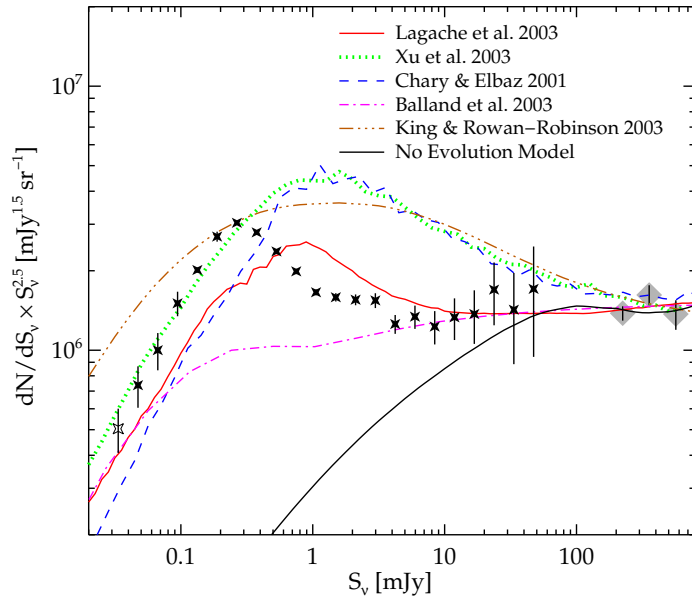


FIGURE 1. Differential *Spitzer* 24 μm number counts (from Papovich *et al.* 2004), normalized to a Euclidean slope, $dN/dS_\nu \sim S_\nu^{-2.5}$. The solid stars show the average counts from all the *Spitzer* fields. Each flux bin is $\Delta(\log S_\nu) = 0.15$ dex. The shaded diamonds correspond to *IRAS* 25 μm number counts from Hacking & Soifer (1991). The curves show the predictions from various contemporary models from the literature (see figure inset; and adjusted slightly to match the observed *IRAS* counts), and a model based on the local *ISO* 15 μm luminosity function and assuming non-evolving galaxy SEDs.

instrument are key because of their sensitivity to IR emission and angular resolution (see Rieke *et al.* 2004). Deep, large-area surveys with *Spitzer* are currently underway, and early results demonstrate that *Spitzer*–selected IR–luminous galaxies are not only common at high–redshifts ($z \gtrsim 1$; e.g. Le Floc'h *et al.* 2004), but may bridge the gap between the far–IR/sub-mm galaxy populations at $z \sim 3$ and galaxies at more moderate redshifts — placing them in the context of the cosmic star–formation–rate density (e.g. Egami *et al.* 2004).

In these proceedings, we present early results from IR surveys with *Spitzer* at 24 μm from time allocated to the Guaranteed Time Observers (GTOs), and we consider implications for IR–stages of galaxy evolution. We then describe the properties of 24 μm –selected galaxies using deep ground–based and *HST* imaging, and we discuss questions that arise when considering IR–luminous galaxies within contemporary theories of galaxy evolution. Wherever appropriate, we assume a cosmology with $H_0 = 70 \text{ km s}^{-1} \text{ Mpc}^{-1}$, $\Omega_m = 0.3$, and $\Lambda = 0.7$.

2. *Spitzer* Observations of Distant IR–Luminous Galaxies

Spitzer provides efficient, deep observations of large areas of sky containing a high source surface density. Figure 1 shows the 24 μm differential number counts that have been derived using roughly 50,000 galaxies from five fields spanning approximately 10.5 square degrees (Papovich *et al.* 2004). At bright flux densities, $S_\nu \gtrsim 5 \text{ mJy}$, the differential 24 μm source counts increase at approximately the Euclidean rate, $dN/dS_\nu \sim S_\nu^{-2.5}$,

which extends the trends observed by the IRAS 25 μm population by two orders of magnitude (Hacking & Soifer 1991; Shupe *et al.* 1998). For $S_\nu \simeq 0.4 - 4$ mJy, the counts increase at a super-Euclidean rate, and peak near 0.2 – 0.4 mJy. This observation is similar to the trend observed in the *ISO* 15 μm source counts (Elbaz *et al.* 1999), but the peak in the 24 μm differential source counts occurs at fluxes fainter by a factor ≈ 2.0 . The counts converge rapidly at $\lesssim 0.2$ mJy, with a faint-end slope of $dN/dS_\nu \sim S_\nu^{-1.5 \pm 0.1}$.

The thick line in figure 1 shows the expected counts from non-evolving models of the local IR-luminous population. While the non-evolving fiducial model is consistent with the observed 24 μm counts for $S_\nu \gtrsim 20$ mJy, it underpredicts the counts at $S_\nu \lesssim 0.4$ mJy by more than a factor of 10. The *Spitzer* 24 μm number counts require strong evolution in the IR-luminous galaxy population. This is similar to conclusions based on data from *IRAS* and *ISO*, but the *Spitzer* counts extend them to fainter fluxes (and higher redshifts, see below) than those probed from these earlier missions.

2.1. Interpretation of 24 μm sources

The 24 μm source counts differ strongly from predictions of various contemporary models (as labeled in figure 1). Four of the models are phenomenological in approach (so-called ‘backwards-evolution’ models), which evolve the parameters of the local luminosity function back in time (generally accounting for density and luminosity evolution by changing ϕ^* and L^*) to match counts from *ISO*, radio, sub-mm, and other datasets. Several models (Chary & Elbaz 2001; King & Rowan-Robinson 2001; Xu *et al.* 2003) show a rapid increase in the number of sources with super-Euclidean rates at relatively bright flux densities ($S_\nu \gtrsim 10$ mJy). They predict 24 μm counts that peak near 1 mJy, and overpredict the measured counts at this flux density by factors of 2 – 3. These models expected there to be more luminous IR galaxies (LIRGs) and ultra-luminous IR galaxies (ULIRGs) selected by *Spitzer* 24 μm near $z \sim 1$, based largely on the redshift distribution of the *ISO* 15 μm sources. Lagache *et al.* (2003) predicted roughly Euclidean counts for $S_\nu > 10$ mJy. The shape of the counts in this model is similar to the observed distribution, but it peaks at $S_\nu \sim 1$ mJy, at higher flux densities than the observed counts. This model has a redshift distribution that peaks near $z \sim 1$, but tapers somewhat slower with a significant population 24 μm sources out to $z \gtrsim 2$ (Dole *et al.* 2003).

The peak in the 24 μm differential number counts occurs at fainter flux densities than predicted from the models based on the ISO results. Because the number counts are essentially just the integral of the galaxy luminosity function over redshift and flux down to the survey flux limit, they are likely dominated by galaxies with ‘ L^* ’ luminosities (modulo variations in the faint-end slope of the luminosity function). Models that reproduce the IR background require far-IR luminosity functions with $L^*(\text{IR}) \gtrsim 10^{11} L_\odot$ (see Hauser & Dwek 2001). Elbaz *et al.* (2002) observed that the redshift distribution of objects with these luminosities in deep *ISO* 15 μm surveys spans $z \simeq 0.8 - 1.2$, and that these objects constitute a large fraction of the total cosmic IR background. Assuming the 24 μm number counts at 0.1 – 0.4 mJy correspond to L^* galaxies, their redshifts must lie at $z > 1$.

2.2. Challenges to Galaxy Evolution Theories

Recently, Lagache *et al.* (2004) have updated their phenomenological model in order to reproduce the measured *Spitzer* number counts. To do this, they required a minor modification of the redshift distribution of 24 μm sources, such that galaxies with $z \gtrsim 1$ contribute more than half of the counts at faint fluxes (~ 0.2 mJy). They also required an adjustment to the flux density in the mid-IR region of galaxy SEDs (3 – 30 μm) of up to a factor of two. The implications are: 1) that stochastically heated emission

features at mid-IR wavelengths (UIBs and PAHs) likely persist at high redshifts ($z \gtrsim 2$); and 2) the relative strength of the various mid-IR features may evolve with redshift. The second implication is not wholly unexpected as higher redshift galaxies may have very different metallicity and chemistry, and the cosmic UV radiation field is more intense (the latter contributes to the heating of the grains responsible for the mid-IR emission features, e.g. Désert *et al.* 1990). The intriguing prospect is that the mid-IR SEDs of IR-luminous galaxies may evolve with redshift, which complicates modeling efforts. Forthcoming spectroscopy of high-redshift galaxies at mid-IR wavelengths with the *Spitzer* Infrared Spectrograph will measure the strength of these features and will help to constrain any evolution observationally.

Although backwards-evolution models provide a useful framework for parameterizing the strong evolution of IR-luminous galaxies, they are unable to explain the physics responsible for this evolution. Models of galaxy formation and evolution that start from first principles (so called ‘forward-evolution’ models) currently lack the means of producing either the strong evolution observed in the IR number counts or in the cosmic IR background (see, e.g. Hauser & Dwek 2001). For example, the dot-dashed line in figure 1 shows the model of Balland, Devriendt, & Silk (2003), which is based on semi-analytical hierarchical models within the Press-Schechter formalism. In that model, galaxies identified as ‘interacting’ are assigned IR-luminous galaxy SEDs. This model includes additional physics in that the evolution of galaxies depends on their local environment and merger/interaction histories. Although this model predicts a near-Euclidean increase in the counts for $S_\nu \gtrsim 10$ mJy, the counts shift to sub-Euclidean rates at relatively bright flux densities. Semi-analytic models by R. Somerville, J. Primack, *et al.* (in preparation), which broadly reproduce optical-near-IR properties of galaxies from $z \sim 0-3$, predict an IR background intensity that is too faint by several factors. These examples are typical of the general status of forward-evolution modeling efforts. *We are faced with a lack of understanding why such rapid evolution occurs in the IR-luminous galaxy population.*

3. Ground-based Observations of Distant *Spitzer* Galaxies

The *Spitzer* GTO extragalactic survey fields were selected to have low zodiacal and Galactic backgrounds (see § 5; table 1), and to have the highest-quality ancillary data available at other wavelengths. The GTOs used *Spitzer* to observe a 1×0.5 sq. degree region of *Chandra* Deep Field South (CDF-S) in early February 2004. The CDF-S has exceptional ancillary data from X-ray to radio wavelengths. For the remainder of this contribution we will discuss only a portion of these data — focusing on the optical imaging and redshift distribution of the *Spitzer*-selected galaxies. Studies of the *Spitzer* sources in this field using other ancillary data have been carried out or are in progress. For example, Rigby *et al.* (2004) study the properties of X-ray-selected *Spitzer* 24 μ m sources in this field.

The region around the CDF-S has been the target of several ground-based imaging surveys. Of these, the COMBO-17 survey (Classifying Objects by Medium-Band Observations in 17 filters; Wolf *et al.* 2003) has observed a 30×30 sq. arcmin region around the CDF-S field with imaging from $0.3 - 1 \mu$ m. Using a suite of medium-band filters, they provide highly-reliable photometric redshifts for galaxies with $R \leq 24$ to $z \lesssim 1.3$, and for AGN out to substantially higher redshift (Wolf *et al.* 2004). Nearly the entire COMBO-17 field overlaps with the *Spitzer* field. Most *Spitzer* 24 μ m sources brighter than 60 μ Jy (the estimated 50% completeness limit) are readily identified in the COMBO-17 images: 3850 of the 4720 24 μ m sources in this region have optical counterparts to $R \leq 25$ within 2'' (the *Spitzer* 24 μ m PSF is roughly 6'' FWHM). Of these, roughly 2970 have good

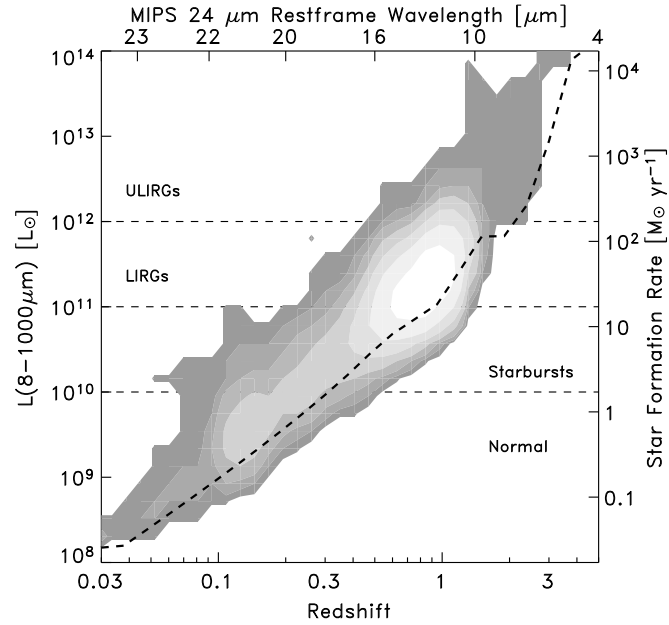


FIGURE 2. Redshift and luminosity distribution of optically-selected *Spitzer*/MIPS 24 μm sources. Redshifts correspond to values published for the COMBO-17 survey (Wolf *et al.* 2004), with additional spectroscopic redshifts from VLT/FORS2 (Vanzella *et al.* 2004) and VIRMOS (Le Fervé *et al.* 2004). Contours indicate regions containing 1, 2, 4, 8, 16, 32, and 64 galaxies in bins of $\Delta \log L(\text{IR}) = 0.2$ and $\Delta \log z = 0.06$. The heavy, dashed line shows the estimated 80% completeness limit of the 24 μm imaging (see Papovich *et al.* 2004). The right-hand axis shows the SFR corresponding to $L(8 - 1000\mu\text{m})$ for the assumption that all the IR luminosity results from star formation, and using the relation established by Kennicutt (1998). The top axis shows the rest-frame wavelength observed at 24 μm . Regions separated by dashed lines show fiducial IR-galaxy classes.

photometric redshift estimates. Several large spectroscopic surveys from the VLT (Le Fervé *et al.* 2004; Vanzella *et al.* 2004) provide an additional 290 *Spitzer* 24 μm sources.

3.1. The redshift distribution of *Spitzer* 24 μm sources

Figure 2 shows the redshift and luminosity distribution of *Spitzer*-selected sources with counterparts in the photometric- and spectroscopic-redshift catalogs from the CDF-S. The total IR luminosity, $L(8 - 1000\mu\text{m})$, is calculated by converting the measured 24 μm flux density to a luminosity using the reported redshift, then extrapolating to the total IR luminosity using the semi-empirical SEDs of Dale *et al.* (2001). It is important to note that there is some scatter between far-IR colors and total IR luminosity, which is not included in the figure (see Chapman *et al.* 2003). Much of this scatter can be reduced by including *Spitzer* 70 μm data to constrain the mid-to-far-IR ‘color’ (see, e.g. Papovich & Bell 2002).

IR-luminous galaxies are readily identified out to $z \sim 1.3$. Galaxies at higher redshifts generally lie beyond the COMBO-17 limits. At low redshifts ($z \lesssim 0.2$) most of the 24 μm -selected sources correspond to relatively normal star-forming galaxies with some starbursts. This reflects the limited volume probed by the survey for these redshifts ($\sim 14000 \text{ Mpc}^3$), in which few IR-luminous galaxies are expected. The majority of 24 μm

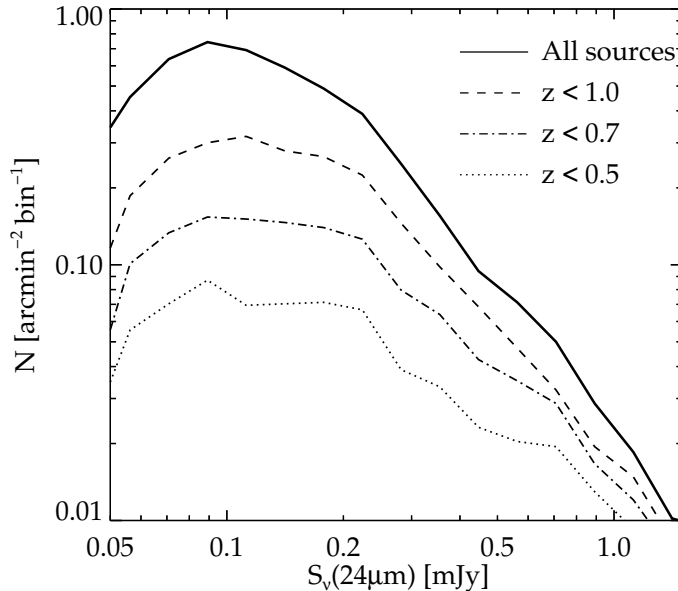


FIGURE 3. Differential *Spitzer* 24 μm number counts in the region of the CDF-S field covered by COMBO-17, which covers roughly 900 sq. arcmin. The solid curve shows the counts from all 24 μm sources in this area. The broken lines show the contribution to the counts from optically-selected galaxies with redshifts below 0.5 (dotted line), 0.7 (dot-dashed line), and 1.0 (dashed line). Each bin is $\Delta(\log S_\nu) = 0.1$ dex. Optically selected IR galaxies with redshifts $z < 1.0$ contribute roughly half of the 24 μm source counts at the faint end (0.1 – 0.4 mJy).

sources with $z \sim 0.4 - 1$ correspond to LIRGs, and these sources likely dominate the IR luminosity density at these redshifts. ULIRGs are generally not common in this field until $z \gtrsim 0.8$, and LIRGs generally seem to dominate the IR emission at these redshifts as well. ULIRGs appear scarce even at these high redshifts, although we are certainly missing optically faint ULIRGs with $R \gtrsim 24$ (see, e.g. Egami *et al.* 2004). To study their properties will require both large survey areas and deep optical data.

Figure 3 shows the 24 μm differential number counts in the *Spitzer*–COMBO-17 overlap areas, and the contribution of galaxies as a function of redshift. At the bright end, most of the counts are due to galaxies with $z \lesssim 1$. At fainter 24 μm flux densities, higher-redshift galaxies dominate the counts. Galaxies with $z \lesssim 0.7$ make up only one-quarter to one-third of the total counts at ~ 0.2 mJy (near the peak in figure 1). Similarly, 24 μm sources at these flux densities with $z \lesssim 1$ contribute only $\sim 50\%$ of the total counts. There is roughly one *Spitzer* 24 μm source per sq. arcmin with no counterpart in the optical images to $R \sim 25$. Elbaz *et al.* (2002) found a redshift distribution of *ISO* 15 μm sources with a median at $z \sim 0.7$ and a small tail to $z \sim 1$. In contrast, the *Spitzer* 24 μm data is very sensitive to galaxies at $z \gtrsim 1$. *The ISO populations make up only a fraction of the faint 24 μm sources.*

3.2. Evolution of the IR-luminosity density

The available redshifts allow a crude estimate for the evolution in the IR luminosity density relative to that in rest-frame UV and visible bands in the CDF-S. From $z \sim$

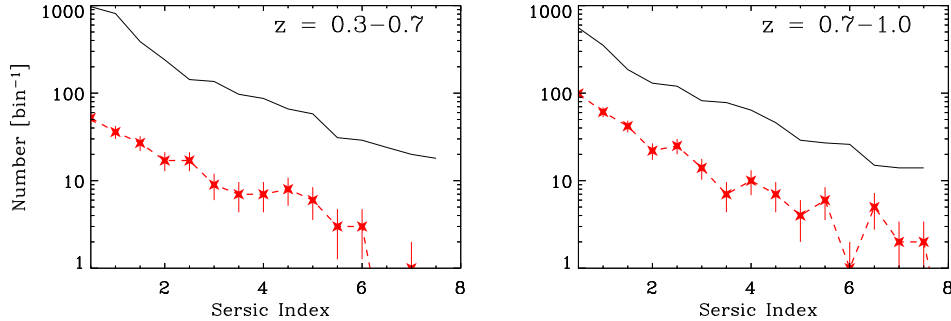


FIGURE 4. Distribution of Sersic indices for GEMS-selected galaxies based on two-dimensional fits to the F850LP images (see Peng *et al.* 2002). The panels show the distribution for galaxies with redshifts between $z = 0.3 - 0.7$ and $z = 0.7 - 1.0$ (as labeled). The stars connected by dashed lines show the distribution of Sersic indices for IR-luminous galaxies with $L_{\text{IR}} > 10^{10.5} L_{\odot}$. The IR-luminous galaxies show approximately the same distribution of Sersic indices as the general galaxy population in both redshift intervals, which suggests that these morphological parameters are not indicative of IR-active stages of galaxy evolution.

0.2 – 1, the luminosity density in the rest-frame U and V bands increases by roughly a factor ~ 3 (uncorrected for extinction effects or incompleteness effects), consistent with findings from previous studies (e.g. Lilly *et al.* 1996). In comparison, the IR luminosity density grows by roughly a factor $\gtrsim 8$, where the inequality symbol denotes the fact that this estimate does not include the contribution from IR-luminous galaxies fainter than the magnitude limits ($R \sim 24$) of the ground-based surveys. This underlines the fact that *the IR-luminous galaxy population appears to evolve more rapidly than that directly measured from UV/optical-selected galaxies*.

4. *HST* Observations of Distant *Spitzer* Galaxies

The Advanced Camera for Surveys (ACS) has greatly improved the efficiency of imaging with *HST*. The region of the CDF-S has extensive *HST*/ACS imaging from the Galaxies Evolution through Morphologies and SEDs survey (GEMS; Rix *et al.* 2004), which provides F606W and F850LP imaging over roughly 780 sq. arcmin, i.e., most of the COMBO-17 field.† To date, *HST* is the most efficient means of obtaining kpc-scale resolution of distant galaxies, as terrestrial adaptive-optics techniques are currently only effective over small patches of sky. Combined with the high-quality redshifts, these wide-area ACS data allow us to test whether structural properties and environmental effects correlate with IR-luminous stages of galaxy evolution.

What is the distribution of galaxy morphological types that are in IR-active evolutionary stages? As a first experiment, one can parameterize morphological type from the *HST* images simply in terms of the Sersic index, n_s (also called the generalized de Vaucouleur profile), where $I(R) \sim \exp(-R^{1/n_s})$. Objects with exponential surface brightness profiles have Sersic indices $n_s \sim 1$, which is typical of disk-like galaxies. Objects with more concentrated surface-brightness profiles have higher Sersic indices, as in the case of spheroids and bulges. Classical $r^{1/4}$ -law galaxies have $n_s = 4$. Crudely speaking the Sersic index quantifies the bulge-to-disk ratio of a galaxy's light emission, and it can be used

† The Great Observatories Origins Deep Survey has deeper ACS imaging in a smaller 160 sq. arcmin area within the GEMS field; see Giavalisco *et al.* (2004).

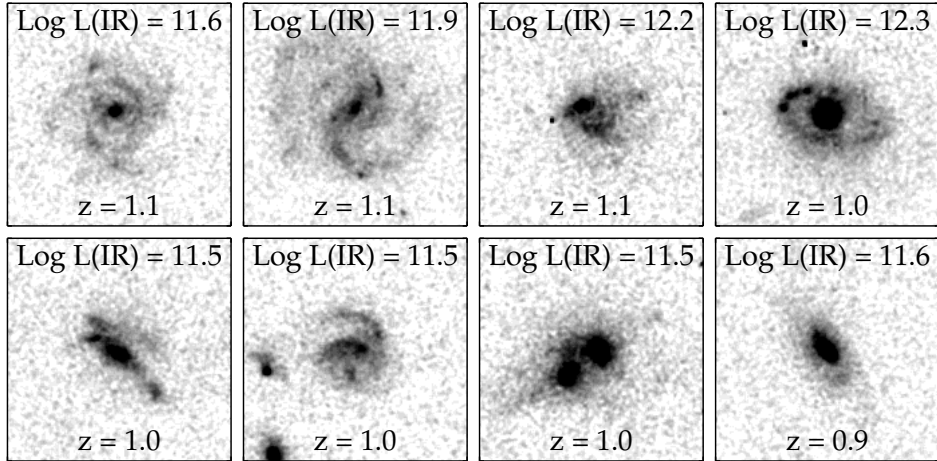


FIGURE 5. ACS F850LP images of luminous IR galaxies at $z \sim 1$ in the CDF-S/GEMS areas. Each image is 5 arcsec per side, which is roughly 40 kpc at these redshifts. Total IR luminosities are given in units of $\log L_{\odot}$. The galaxies have a wide range of morphologies. Clear distortions are evident (the two bottom, leftmost galaxies), including rings (upper rightmost galaxy), and multiple nuclei (second from right, bottom row). However, the two leftmost galaxies on the top row appear to be fairly regular late-type spirals, and the right-most galaxy on the bottom row appears to have a normal spheroidal component.

to discriminate between late-type, disk-dominated galaxies ($n_s \leq 2.5$), and early-type, bulge-dominated galaxies ($n_s > 2.5$).

Figure 4 shows the distribution of Sersic indices for all galaxies in the GEMS catalogs with redshifts $z = 0.3 - 0.7$ and $0.7 - 1.0$. The distribution is skewed towards large numbers of galaxies with lower Sersic indices, which illustrates the fact that the majority of galaxies are disk-dominated. *Interestingly, the distribution of Sersic indices for the IR-luminous galaxies, $L_{\text{IR}} \geq 10^{10.5} L_{\odot}$, is nearly identical to that of the general galaxy population regardless of redshift.* The implication is that these morphological indicators alone are a poor discriminator of IR-activity.

Even the most luminous IR galaxies, $L_{\text{IR}} \gtrsim 10^{11.5} L_{\odot}$, span a range of morphological type. As an illustration, figure 5 shows the ACS/F850LP images of several fiducial IR-luminous galaxies at $z \sim 1$ from the GEMS data. At these redshifts the F850LP filter probes roughly the rest-frame B -band of these galaxies. It is clear that while many of these types of galaxies have highly disturbed morphologies or evidence of strong mergers, there are also clear examples of fairly normal galaxy types. Systematic studies using these data at $z \sim 0.7$ (E. Bell *et al.* in preparation), and as a function of IR-luminosity (C. Papovich *et al.*, in preparation) will help to understand the relation between galaxy morphology, environment, and IR-activity.

5. Selection of Deep, Extragalactic Survey Fields

We close with a discussion on how to choose the location of deep fields for studying IR-luminous galaxies. The dominant sources of IR background are zodiacal light and emission from cirrus clouds in the Milky Way. Zodiacal light dominates at mid-IR wave-

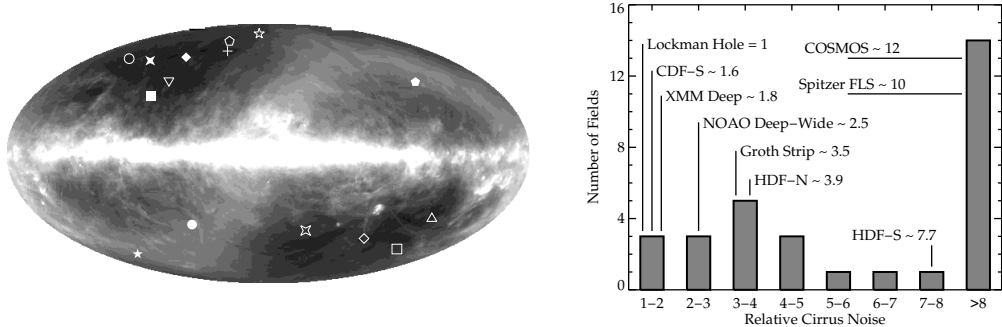


FIGURE 6. *Left*: Location of selected extragalactic survey fields on the Galactic *IRAS* 100 μm image. Galactic north is up, and east to the left. Galactic cirrus dominates the image, although zodiacal emission is evident and runs roughly from the bottom left to the upper right. The symbols denote fiducial fields: HDF-N, *filled star*; HDF-S, *open star*; CDF-S, *open square*; Marano, *open diamond*; XMM-Deep, *open pentagon*; XMM-LSS, *filled pentagram*; NOAO Boötes, *cross*; Groth strip, *filled diamond*; ELAIS-N1, *downward triangle*; ELAIS-S2, *upward triangle*; COSMOS, *pentagon*; Lockman Hole, *open circle*; SSA22, *filled circle*; Subaru Deep, *open pentagram*; Spitzer FLS, *filled square*. *Right*: Far-IR cirrus noise of the extragalactic survey fields listed in table 1 relative to that of the Lockman Hole. Estimates are based on the Galactic $N(\text{HI})$, which correlates linearly with cirrus brightness. High cirrus noise substantially increases the confusion noise at all angular scales and is a strongly limiting factor for far-IR observations.

lengths (3 – 40 μm), decreases rapidly with ecliptic latitude, and shows strong seasonal changes (e.g. Price *et al.* 2003). Galactic cirrus is the dominant source of background at far-IR wavelengths (40 – 200 μm). It scales roughly linearly with the Galactic column density, $N(\text{HI})$ (Lockman *et al.* 1986; Boulanger & Perault 1988), and produces two noise components for IR observations. The first is due simply to the elevated sky brightness, which limits the flux sensitivity of an observation by a factor roughly $\sim \sigma_{\text{cirrus}}^{-1}$. Fields near the plane will require exposures several times longer than fields near the poles to achieve comparable depth.

The second component is confusion noise from structure within cirrus clouds (e.g. Low *et al.* 1984; Helou & Beichman 1990; Kiss *et al.* 2001, 2003). Helou & Beichman expressed the cirrus confusion noise as $\sigma_{\text{cirrus}} \sim \lambda^{2.5} D^{-2.5} B_{\lambda}^{1.5}$, where λ is the emitted wavelength, D is the diameter of the telescope aperture, and B_{λ} is the mean sky brightness. Because cirrus brightness correlates with Galactic hydrogen column density, an increase in $N(\text{HI})$ by a factor of five corresponds to an increase in the relative confusion noise by a factor of ten. Far-IR observations in fields with high cirrus sky brightness pay a substantial penalty in terms of cirrus-confusion noise, and this imposes a hard limit on the ultimate survey depth in such fields.

Table 1 lists the properties of known extragalactic survey fields (updated and adapted from a compilation by Stiavelli *et al.* 2003). For each field, the Galactic extinction (parameterized by the color excess, $E(B - V)$) and hydrogen column density are taken from the maps of Schlegel *et al.* (1998) and Dickey & Lockman (1990), respectively. The left panel of figure 6 shows the location of several of these fiducial fields superimposed on an *IRAS* 100 μm all-sky image. The right panel of figure 6 shows the distribution of Galactic cirrus confusion noise relative to that of the Lockman Hole, the sightline with the minimum $N(\text{HI})$.

Fields that are both far from the ecliptic (low zodiacal light) and the Galactic plane (low $N(\text{HI})$ and cirrus) have the lowest backgrounds and confusion noise, and are, in a sense, chosen by nature to be the ideal locations for full multi-wavelength extragalactic surveys.

Compilation of the Properties of Known Extragalactic Survey Fields.						
Name	R.A. (J2000.0)	Decl. (J2000.0)	<i>l</i> (deg)	<i>b</i> (deg)	<i>E(B–V)</i>	<i>N(HI)</i> (10^{20}cm^{-2})
DEEP-1	0:17:00	16:00:00.0	111.0	-46.1	0.049	4.18
WHT Deep	0:22:33	00:20:57.0	107.6	-61.7	0.025	2.73
ELAIS-S1	0:34:44	-43:28:12.0	313.5	-73.3	0.008	2.52
FORS Deep	1:06:04	-25:45:46.0	191.1	-86.5	0.018	1.88
XMM-LSS	2:21:20	-04:30:00.0	170.3	-58.8	0.027	2.61
CNOC2	2:23:00	00:00:00.0	165.7	-55.1	0.039	2.96
DEEP-2	2:30:00	00:00:00.0	168.1	-54.0	0.022	2.89
CFDF	3:00:00	00:00:00.0	177.0	-48.9	0.096	6.99
Marano	3:15:09	-55:13:57.0	270.2	-51.8	0.016	2.45
CDF-S [†]	3:32:30	-27:48:47.0	223.6	-54.4	0.008	0.79
ELAIS-S2	5:02:24	-30:35:55.0	232.6	-35.7	0.012	1.43
CNOC2	9:20:00	37:00:00.0	186.6	44.7	0.011	1.47
COSMOS	10:00:29	02:12:21.0	236.8	42.1	0.017	2.90
Lockman Hole [†]	10:52:43	57:28:48.0	149.3	53.1	0.008	0.57
EIS Deep	11:20:45	-21:42:00.0	276.4	36.5	0.045	4.18
HDF-N [†]	12:36:49	62:12:58.0	125.9	54.8	0.012	1.41
SSA13	13:12:21	42:41:21.0	109.0	73.9	0.014	1.46
Subaru Deep	13:24:21	27:29:23.0	37.6	82.7	0.019	1.19
XMM Deep [†]	13:34:37	37:54:44.0	85.6	75.9	0.006	0.83
Groth Strip [†]	14:16:00	52:10:00.0	96.3	60.4	0.013	1.30
ELAIS-N3	14:29:06	33:06:00.0	54.7	68.1	0.008	1.11
NOAO Boötes [†]	14:32:06	34:16:47.5	58.2	67.7	0.012	1.04
ELAIS-N1	16:10:01	54:30:36.0	84.3	44.9	0.005	1.38
ELAIS-N2	16:36:58	41:15:43.0	65.3	42.2	0.007	1.07
DEEP-2	16:52:00	34:55:00.0	57.4	38.3	0.016	1.78
<i>Spitzer</i> FLS	17:18:00	59:30:00.0	88.3	34.9	0.023	2.66
CFHT Legacy	22:15:31	-17:44:05.0	39.3	-52.9	0.026	2.39
SSA22	22:17:35	00:15:30.0	63.1	-44.0	0.066	4.64
DEEP-2	23:30:00	00:00:00.0	85.0	-56.7	0.037	4.04
HDF-S	22:32:56	-60:30:02.7	328.3	-49.2	0.027	2.22
EIS Deep	22:50:00	-40:12:59.0	357.5	-61.7	0.011	1.47

[†] Denotes field included in the *Spitzer* GTO cosmological surveys.

Future IR missions (e.g. JWST, Herschel, SAFIR) will gravitate to these fields, as well as future X-ray telescopes (e.g. Constellation–X). To optimally study IR–luminous stages of galaxy evolution will require full panchromatic surveys in these fields, including high–angular *HST* imaging. These multi–wavelength data will be crucial for dissecting the mechanisms for galaxy evolution, not only in the *Spitzer* era, but for decades to come.

We are indebted to all our collaborators on this project for their work and for allowing us to present some of this material prior to publication. We wish to acknowledge the fellow members of the *Spitzer* MIPS, IRAC, and IRS GTO teams for stimulating conversations, efficient processing and analysis of the data, and much hard work. We would also like to thank the members of the COMBO–17 and GEMS teams for their assistance and useful conversations, in particular Eric Bell, Dan McIntosh, Hans–Walter Rix, Rachel Somerville, and Christian Wolf. C.P. acknowledges highly interesting conversations with other participants at the Aspen Center for Physics, where much of this work

was completed. Finally, we would like to extend our deep appreciation to the symposium organizers for the invitation to present this material, and for planning such an interesting and successful meeting. Support for this work was provided by NASA through contract 960785 issued by JPL/Caltech.

REFERENCES

Balland, C., Devriendt, J. E. G., & Silk, J. 2003, MNRAS, 343, 107

Chapman, S. C., Helou, G., Lewis, G. F., & Dale, D. A. 2003, ApJ, 588, 186

Chary, R. R., & Elbaz, D. 2001, ApJ, 556, 562

Dale, D. A., Helou, G., Contursi, A., Silbermann, N. A., & Kolhatkar, S. 2001, ApJ, 549, 215

Désert, F.-X., Boulanger, F., & Puget, J.-L. 1990, A&A, 237, 215

Dickey & Lockman, 1990, ARAA, 28, 215

Dole, H., Lagache, G., & Puget, J.-P. 2003, ApJ, 585, 617

Egami, E., *et al.* 2004, ApJS, in press (astro-ph/0406359)

Elbaz, D., *et al.* 1999, A&A, 351, L37

Elbaz, D., *et al.* 2002, A&A, 384, 848

Franceschini, A., Aussel, H., Cesarsky, C. J., Elbaz, D., & Fadda, D. 2001, A&A, 378, 1

Giavalisco, M., *et al.* 2004, ApJL, 600, L93

Hacking, P., & Soifer, B. T. 1991, ApJ, 367, L49

Hauser, M. G., *et al.* 1998, ApJ, 508, 25

Hauser, M. G. & Dwek, E. 2001, ARAA, 39, 249

Helou, G. & Beichman, C. A. 1990, in *From Ground-Based to Space-Borne Sub-mm Astronomy*, ed. B. Kaldeich (Noordwijk: ESA), 117

Kennicutt, R. C., Jr. 1998, ApJ, 498, 541

King, A. J., & Rowan–Robinson, M. 2003, MNRAS, 339, 260

Kiss, Cs., Ábrahám, P., Klaas, U., Juvela, M., & Lemke, D. 2001, A&A, 379, 1161

Kiss, Cs., *et al.* 2003, A&A, 399, 177

Lagache, G., Dole, H., & Puget, J.-L. 2003, MNRAS, 338, 555

Lagache, G., *et al.* 2004, ApJS, in press (astro-ph/0406016)

Le Floc'h, E., *et al.* 2004, ApJS, in press (astro-ph/0406148)

Low, F. J., *et al.* 1984, ApJL, 278, L19

Papovich, C. & Bell, E. F. 2002, ApJ, 579, L1

Papovich, C., *et al.* 2004, ApJS, in press, (astro-ph/0406035)

Peng, C. Y., Ho, L. C., Impey, C. D., & Rix, H.-W. 2002, AJ, 124, 266

Price, S. D., Noah, P. V., Mizuno, D., Walker, R. G., & Jayaraman, S. 2003, AJ, 125, 962

Rieke, G. & Low, F. 1972, ApJ, 176, 95

Rieke, G., *et al.* 2004, ApJS, in press

Rigby, J., *et al.* 2004, ApJS, in press (astro-ph/0406029)

Rix, H.-W., *et al.* 2004, ApJS, 152, 163

Sanders, D. B., *et al.* 1988, ApJ, 325, 74

Schlegel, D. J., Finkbeiner, D. P., & Davis, M. 1998, ApJ, 500, 525

Shupe, D. L., Fang, F., Hacking, P. B., & Huchra, J. P. 1998, ApJ, 501, 597

Soifer, B. T., Neugebauer, G., & Houck, J. R. 1987, ARAA, 25, 187

Soifer, B. T., & Neugebauer, G. 1991, AJ, 101, 354

Stiavelli, M., Panagia, N., & Ferguson, H. 2003, *Field Selection Criteria for the ACS Ultra Deep Field* (www.stsci.edu/hst/udf/planning_doc_files/field2)

Vanzella, E., *et al.* 2004, A&A, submitted (astro-ph/0406591)

Wolf, C., Meisenheimer, K., Rix, H.-W., Borch, A., Dye, S., & Kleinheinrich, M. 2003, A&A, 401, 73

Wolf, C., *et al.* 2004, A&A, 421, 913

Xu, C., Lonsdale, C. J., Shupe, D. L., Franceschini, A., Martin, C., & Schiminovich, D. 2003, ApJ, 587, 90